Title

Independent origins of spicules reconcile palaeontological and molecular evidence of sponge evolutionary history

Authors

Maria Eleonora Rossi[1,2,3], Joseph N. Keating[1], Nathan James Kenny[3,4], Mattia Giacomelli[1,5], Sandra Álvarez-Carretero[1], Astrid Schuster[6], Paco Cárdenas[7,8], Sergi Taboada[3,9,10,11], Vasiliki Koutsouveli[3,12], Philip Donoghue[1*], Ana Riesgo[3,9,10*] and Davide Pisani[1*]

Affiliations

1 - Bristol Palaeobiology Group, School of Earth Sciences, University of Bristol, Life Sciences Building, Tyndall Avenue, Bristol BS8 1TH, UK

2 - Centre for Chromosome Biology, School of Biological and Chemical Sciences, University of Galway, Galway H91 W2TY, Ireland

3 - Life Sciences Department, The Natural History Museum, London SW7 5BD, UK

4 - Biochemistry Department, School of Biomedical Sciences, University of Otago, Dunedin, Aotearoa New Zealand

5 - Departament de Genetica, Facultat de Biologia, Universitat de Barcelona, Diagonal 645, 08028 Barcelona, Spain

6 - Department of Biology, University of Southern Denmark, Nordcee, Campusvej 55, Odense M 5230, Denmark

7 - Pharmacognosy, Department of Medicinal Chemistry, Uppsala University, Husargatan 3, Uppsala 751 23, Sweden

8 - Museum of Evolution, Uppsala University, Norbyvägen 16, Uppsala 752 36, Sweden

9 - Department of Biodiversity and Evolutionary Biology, National Museum of Natural Sciences (CSIC), c/José Gutiérrez Abascal 2 28006 Madrid, Spain

10- Departamento de Biodiversidad, Ecología y Evolución, Facultad de Ciencias, Universidad Complutense de Madrid, Madrid, Spain

11- Departamento de Ciencias de la Vida, EU-US Marine Biodiversity Group, Universidad de Alcalá, Alcalá de Henares, Spain

12 - Division of Marine Ecology, Marine Evolutionary Ecology, GEOMAR Helmholtz Centre for Ocean Research Kiel, Kiel, Germany

*Corresponding authors: Philip C.J. Donoghue (Phil.Donoghue@bristol.ac.uk), Ana Riesgo (anariesgogil@mncn.csic.es), and Davide Pisani (davide.pisani@bristol.ac.uk).

Abstract

Sponges (Porifera) are ecosystem engineers playing a critical role in global biogeochemical processes. Their evolution is key to clarify Neoproterozoic paleoecology but remains mired in controversy. Molecular timescales suggest a Tonian or Cryogenian origin while their oldest unequivocal fossils consist of disarticulated siliceous spicules from the Late Ediacaran. We derived a new, dated sponge phylogeny and tested whether ancestral sponges had mineralized skeletons. We resolve the sponge phylogeny in good agreement with current knowledge but date their origin to the early Ediacaran, rather than the Cryogenian or Tonian. We show that early sponges were uncapable of biomineralization and both biosilicification and biocalcification evolved independently multiple times across Porifera. Our results reconcile fossil and molecular estimates of sponge evolution, by showing than their Neoproterozoic history is limited to the Ediacaran, but they are largely absent from the Ediacaran fossil record because they were yet to evolve biomineralized skeletons.

Introduction

The sponge animal phylum (Porifera) is composed of four extant lineages (Calcarea, Homoscleromopha, Demospongiae and Hexactinellida) sharing a bodyplan characterized by a system of pores (ostia) and channels that allow water to circulate through them. Sponges provide key ecosystem services, from habitat formation to nutrient and silica cycling, water filtering and substrate stabilization (*1*). Phylogenetically, sponges are either the sister group of all the other animals or else the second phylum to branch from the animal crown-ancestor (*2–8*). As such, sponges are key to understanding the time of emergence, body plan and ecology of the ancestral animal. However, early sponge evolution is the subject of controversy. Molecular divergence time and fossil biomarker studies have long suggested that sponges diverged in the Tonian or Cryogenian (*9–13*) anticipating a deep Neoproterozoic appearance of sponge fossils. Although there are Tonian, Cryogenian and early Ediacaran fossils with claims of sponge affinity, their interpretations as such range from speculative to contentious

(*14*, *15*). For example, anastomosing pores within Tonian carbonates have been interpreted as keratose sponges (*16*) but corroborative anatomical evidence and a preservational model are lacking, and these structures are more readily interpreted as abiotic sedimentary artefacts (*17*). Late Cryogenian C_{30} steranes (fossil biomarkers) interpreted as evidence for Cryogenian demosponges (24-ipc and 26-mes; (*11*)) have also been interpreted as diagenetically altered C_{29} sterols from chlorophyte algae (*18*). Pores in skeletal fragments from the Cryogenian of South Australia have been interpreted as sponge-like ostia (*19*) but again lack corroborating anatomical evidence, while the middle Ediacaran *Eocyathispongia qiania*, originally interpreted as an adult asconoid sponge (*20*), appears to lack the expected internal structure (*21*, *22*). Finally, arsenopyrite crystal aggregates from the latest Ediacaran of Mongolia (*23*) have been misinterpreted as siliceous sponge spicules (*24*). There is therefore a minimal mismatch of 150 Myr between most molecular estimates for the time of origin of crown sponges and their first unambiguous fossil evidence, represented by disarticulated siliceous spicules from the latest Ediacaran ca. 543 Ma (*14*, *15*, *25*, *26*).

Three sponge lineages (Hexactinellida, Homoscleromorpha and Demospongiae) make spicules out of silicic acid and a series of previous groundbreaking molecular and genomic analyses have shown that they use different biochemical pathways to do so, suggesting that siliceous spicules might have evolved multiple times independently (*27–30*). The fourth sponge lineage, Calcarea, makes spicules using calcite (*31*, *32*). Skeletal elements made of calcium carbonate (but not spicules) are also found in sclerotized demosponges (represented in our dataset by the keratose *Vaceletia*; (*33*)). Some fossil sponges (stomatoporoids) built their skeletons using calcium phosphate, making the sponges the first phylum that could use all three main biominerals (*34*), but there is no evidence of sponges with phosphatic skeletons before the Ordovician. Accordingly, stomatoporoids do not seem relevant to understanding the early fossil record of sponges. Sponges with skeletal elements made of calcite (both Calcarea and Demospongiae) use carbonic anhydrase paralogs to precipitate calcium carbonate (*35–38*). However, carbonic anhydrase paralogs play key role in many cellular functions (including the regulation of intracellular pH (*32*, *35*, *39*)) and these enzymes seem to have been independently recruited into biocalcification pathways multiple times across Metazoa (*35*). Accordingly, the universal distribution of carbonic anhydrase paralogs across Porifera is not surprising, and while the last common sponge crown-ancestor certainly had multiple carbonic anhydrase paralogs (perhaps up to eight (*32*, *38*)), this does not necessarily constitute evidence for a single origin of biocalcification in sponges. Multiple origins of biocalcification would fit better with

the biochemical diversity observed in calcifying sponges for which data are available and their use of alternative carbonic anhydrase paralogs (*31*, *37*, *38*).

While the oldest fossil spicules (ca. 543 Ma; Late Ediacaran) are made of silica (*14*, *25*, *26*), these siliceous spicules only slightly predate a broader diversity of early sponges (Late Ediacaran to early Cambrian) with disparate skeletal structures. These include sponges with a calcareous (aspiculated) skeleton – archaeocyathids (*14*, *40*), biminerallic spicules made of both calcite and silica (e.g. *Eiffelia globosa* (*41*)), and even sponges without skeletal elements, including the late Ediacaran *Helicolocellus cantori* (539 Ma; a stem hexactinellid (*42*)) and *Arimasia germsi* (543-539 Ma; an archaeocyathid (*43*)). Hexactinellida and Archaeocyathida (*15*, *40*) are both crown sponges, and these fossils provide direct evidence that Porifera had a Neoproterozoic history, although its extent is unclear.

Fossil evidence alone paints a confusing picture of early sponge evolution, with a limited Late Ediacaran record composed of a mixture of siliceous spicules and body fossils without skeletal elements, making it difficult to rationalize whether the last common sponge ancestor had a biomineralized skeletons with spicules (*26*), and if it had, whether these spicules were made of silica, calcium carbonate or both (*14*). Alternatively, Ediacaran sponges might have had an aspiculated carbonatic skeleton, similarly to Cambrian Archaeocyathida, or an organic skeleton of axial filaments (similar to some keratose sponges) without biomineralized elements or armed with biomineralized fibers rather than spicules such as is observed in the biosilicified but aspiculated Cambrian sponge *Vauxia* (*44*). Soft bodied sponges with a purely organic skeleton would have had low fossilization potential and could have enjoyed a long, cryptic, Neoproterozoic history, potentially extending to the Cryogenian or the Tonian. This uncertainty leaves the problem of reconciling molecular and fossil evidence for the origin of sponges unresolved.

Here we perform phylogenomic analyses of a new dataset composed of 70 genomes and transcriptomes (12 of which are new to this study). We use our phylogeny to perform molecular clock analyses that integrate new interpretations of the animal fossil record and recent reassessments of key fossil-bearing formations in the rock record (*22*). Finally, we test whether late Ediacaran siliceous spicules could be remains of stem or crown sponges using ancestral state estimation methods. Our ancestral state estimations integrate biochemical, morphological and fossil evidence using structured Markov models of character state transformation with embedded dependencies (*45*, *46*). The hierarchical structure of these models (see Material and Methods and Supplementary Methods in the Supplementary Material – SM) allow testing whether morphological characters underpinned by different

developmental programs (e.g. siliceous spicules underpinned by different biosynthetic pathways) represent independent origins of the same character, or else reflect a deep homology (*47*) where non-homologous gene replacements in an ancestral regulatory network led to the emergence of multiple developmental pathways, the homology of the compared characters notwithstanding (*48*).

Our results indicate that sponges originated in the early Ediacaran (ca. 608 Ma) and that the last common ancestor of all the sponges was not biomineralized and did not possess spicules. Sponges with calcareous skeletons, including calcareous spicules, biminerallic spicules and sclerotized (aspiculated) skeletons, emerged multiple times independently. Calcareous spicules are limited to Calcarea, a lineage that emerged post-Cambrian (473.24 – 157.52 Ma). Siliceous spicules most likely evolved independently multiple times. With reference to living sponges, siliceous spicules evolved once in Homoscleromorpha, once in Hexactinellida and twice in Demospongiae. In Demospongiae, siliceous spicules emerged in the stem to the Heteroscleromorpha clade and in the Verongimorpha genus *Chondrilla*, which is nested within the clade of aspiculate Demospongiae. When fossil taxa are also considered, other independent origins of siliceous spicules are inferred. Nonetheless, the last common ancestor of all sponges is invariably reconstructed as lacking biomineralized skeletal elements. We performed a focal study, using diversification rate shift analyses on the extant Silicea, which represent most extant sponge biodiversity, identifying two potentially significant diversification shifts nested within Heteroscleromorpha, both post-dating the emergence of siliceous spicules. Accordingly, at least in the case of Silicea the emergence of siliceous spicules does not appear to have played a significant role in their diversification.

Our estimates of the timescale of sponge divergence, combined with our study of spicule evolution and previous genomic, biochemical, and palaeontological evidence for the evolution of siliceous spicules (*14*, *27*, *29*, *30*, *42*), suggest that while sponges evolved in the early Ediacaran, contradicting previous analyses calibrated using fossil biomarkers, early sponges lacked spicules or other biomineralized skeletal structures, and had low preservation potential. Sponges had a cryptic, but relatively short, Neoproterozoic history which *de facto* reconciles the sponge fossil record with molecular estimates of divergence times.

Results

Resolving the sponge phylogeny

Orthofinder v. 2.7.1 (*49*) assigned 75% of the 5,657,552 sequences in our dataset to a total of 335,892 orthogroups. This set of orthogroups was filtered (see Materials and Methods and Supplementary Methods in SM) to remove paralogs. We retained only the orthogroups that had 90% of species left after filtering paralogs out. This resulted in 1,468 orthogroups that were further filtered to remove long branched taxa (see Materials and Methods and Supplementary Methods in SM for precise details). A final filtering step was performed to remove families that might be including hidden paralogs (see Materials and Methods and Supplementary Methods in SM for details). Our orthogroup filtering strategy left us with a dataset of 70 species (64 belonging to Porifera) and 133 protein coding genes, that were used for phylogenetic and molecular clock analyses. The 133 protein coding genes were analyzed independently to generate gene trees and as a concatenated superalignment of 103,269 amino acids (AA). The concatenated dataset was analysed using Maximum Likelihood (ML) with the best fitting across-site compositionally homogeneous model in IQTree (*50*) and using Bayesian analysis with the across-site compositionally heterogeneous (CATegories model (*51*) – the CAT–Poisson model) in PhyloBayes (*52*). See (*3, 4, 7*) for the differences between across-site compositionally homogeneous and heterogeneous models. Finally, we used ASTRAL (*53*) with the 133 single gene trees. See https://figshare.com/s/0a33312af1a00d935f85 for the individual single gene alignments, the gene trees and the outputs of all our phylogenetic analyses.

Phylogenomic analyses (see Fig. 1 and figs. S1—S3) unequivocally recovered Porifera to be composed of two sister lineages, Silicea (Hexactinellida plus Demospongiae) and Calcarea plus Homoscleromorpha. We recover Calcarea in ML analyses with Ultrafast Bootstrap Support (UBS)= 100. In Bayesian analyses this clade has Posterior Probability (PP)= 1, and in Astral analyses it has Coalescent Branch Support (CBS)= 1. Homoscleromorpha has UBS= 100; PP= 1; CBS= 0.87. The monophyletic group composed of Calcarea and Homoscleromorpha (UBS= 100; PP= 1; CBS= 0.91), is sister to Silicea (UBS= 100; PP= 1; CBS= 1), a monophyletic group comprising Hexactinellida and Demospongiae. Within Calcarea, we recover the monophyly of Calcinea and Calcaronea (UBS= 100; PP= 1; CBS= 1). In our topologies, the Homoscleromorpha (UBS= 100; PP= 1; CBS= 0.87) is represented by two species from the two families Oscarellidae and Plakinidae, and therefore major relationships were not addressed in detail. We recovered both Demospongiae and Hexactinellida as monophyletic, with full support (UBS= 100; PP= 1; CBS= 1). For the Hexactinellida, sampling only includes representatives from the order Lyssacinosida.

In Demospongiae, Keratosa and Verongimorpha are monophyletic (UBS= 100; PP= 0.99; CBS= 0.24) and sister to the Haplosclerida (UBS= 100; PP= 1; CBS= 1) and Heteroscleromorpha (UBS= 100; PP= 1; CBS= 1). In the Verongimorpha, we recover *Aplysina aerophoba* (Verongiida) as the sister of Chondrillida, where we recover the genus *Halisarca* to be paraphyletic. *Halisarca dujardini* is sister (UBS= 100; PP= 1; CBS= 1) to *H. caerulea* and *Chondrilla caribensis* (UBS= 77; PP= 1; CBS= 1). Within Keratosa, we recover *Dendrilla antarctica* (Dendroceratida) to be the sister to the order Dyctioceratida, which emerges to be monophyletic and fully supported (UBS= 100; PP= 1; CBS= 1). We recover the monophyly of Haplosclerida (UBS= 100; PP= 1; CBS= 1), with *Haliclona penicillata* from the family Chalinidae, being sister to *Amphimedon queenslandica* (family Niphatidae) and *Petrosia ficiformis* (family Petrosiidae), all relationships with full support (UBS= 100; PP= 1; CBS= 1). In the Heteroscleromorpha, the earliest diverging clade is composed of Scopalinida plus Spongillida (UBS= 100; PP= 1; CBS= 1). In Spongillida, the family Spongillidae is paraphyletic with *Ephydatia muelleri* clustering sister to the family Lubomirskiidae, which is monophyletic (UBS= 100; PP= 1; CBS= 1). The order Tetractinellida is monophyletic (UBS= 100; PP= 1; CBS= 1). The suborder Spirophorina represented by the species *Craniella infrequens* is sister to the suborder Astrophorina. Astrophorina is monophyletic, with the family Vulcanellidae sister to the families Ancorinidae + Geodiidae. We recovered Bubarida, as sister to Agelasida, Polymastiida, Tethyida, Clionaida, Suberitida, and Poecilosclerida (UBS= 100; PP= 1; CBS= 0.96). In the Bayesian tree (Fig. 1 and fig. S1), Clionaida and Tethyida formed a monophyletic sister group to Suberitida and Poecilosclerida, respectively, and the order Suberitida is recovered sister (PP= 1) to the order Poecilosclerida. In the ML (fig. S2) and Astral (fig. S3) topologies, Suberitida is sister (UBS= 68; CBS= 0.72) to the clade Clionaida + Tethyida, and Poecilosclerida is sister to these tree orders (UBS= 100; CBS= 1). In both topologies, the poecilosclerids form two major clades, with the first one composed of the carnivorous sponge *Chondrocladia robertballardi* sister to the family Mycalidae. The second clade comprises all the other families of the order Poecilosclerida.

Estimating molecular divergence times of sponge evolution

Molecular divergence times (Fig. 1) were inferred using MCMCtree (*54*) for the Bayesian phylogeny (fig. S1), using 12 fossil constraints (see nodes highlighted with red circle in Fig. 1 and detailed descriptions of all 12 calibrations in the "List of Calibrations and their Justifications" in SM). We calibrated the root to have a hard minimum of 574 Ma and a soft

maximum of 609 Ma. The fossil minimum is based on the earliest occurrence of *Charnia masoni*, in the Drook Formation of Mistaken Point, Newfoundland (*55*), while the maximum is based on the Lantian biota of South China which contains a diversity of macrofossils but no credible metazoans (*56*). A uniform prior was used for this calibration, implying that we maintain an agnostic view of where the root of our phylogeny might lie between these constraints. The maximum on the root node is soft, with 2.5% of the probability density falling outside of the 574 – 609 Ma interval, on the deep side of the distribution. Eumetazoa was assigned a hard maximum of 573 Ma. This value was empirically defined to counter truncation problems in molecular clock analyses (see Methods for details) and a soft minimum of 561 Ma based on age of Bed B in the Bradgate Formation, where the earliest crown-eumetazoan, *Auroralumina attenboroughii*, was recovered. While it was possible to establish minimum constraints for the remaining sponge calibrations (*57*, *58*), it was not possible to justify maximum constraints based on palaeontological, biogeographic or geological evidence. The sponge fossil record, at least in terms of records that can inform calibrations for molecular clock analyses, is based on sites of exceptional fossil preservation. As such, we have no prior expectation of whether the earliest records of various sponge clades (details in SM) represent close approximations of true clade ages. Cauchy distributions with a heavy-tail (see Methods and SM) were used for these calibrations, reflecting lack of knowledge on which to establish maximum clade-age constraints.

Two calibration strategies were used. First, we performed analyses where the oldest known siliceous spicule was used to constrain the crown Heteroscleromorpha clade. We refer to this calibration strategy as the Spiculated Demosponges Node (SDN). We then performed an analysis where the same fossil was used to calibrate the root of Porifera – Spiculated Porifera Node (SPN) strategy. These calibration strategies reflect competing interpretations of the fossil record of siliceous spicules. Under SDN, early siliceous fossil spicules are assumed to represent remains of spicule-bearing demosponges (crown Silicea), as suggested by the morphological similarity between the oldest classifiable siliceous spicules (*18*) and those found in living demosponges. Under SPN, siliceous spicules are assumed to have been present in the last common crown ancestor of Porifera, with the spicule fossil record providing a bound on the origin of sponges. We performed molecular clock analyses under the autocorrelated-rates (AR (*59*)) relaxed-clock model and the independent-rates (IR (*60*)) log-normal relaxed-clock model to assess the impact of both calibration strategies (SDN and SPN), see Materials and Methods and SM for details. For each analysis (i.e., SDN-AR; SDN-IR; SPN-AR; and SPN-IR) we ran six independent chains, sampling from both the prior and the posterior. We checked for

convergence (using in house developed scripts see Materials and Methods, Supplementary Methods in SM and https://doi.org/10.5281/zenodo.11488993 for details) and used the chains that passed our MCMC diagnostics to estimate divergence times (see figs. S4-S6 and table S1 and S2), see Materials and Methods, Supplementary Methods in SM for details. Under SDN, we kept three out of the six chains we ran under both the AR and IR relaxed-clock models (table S1). Under SPN we retained four chains out of six for the AR model and five out of six for IR model (table S2).

Results inferred using the two relaxed-clock models and different calibration strategies did not differ significantly; we therefore focus on the results obtained with the SDN-IR analysis. Results from all other analyses are presented in SM (fig. S7-S9; tables S3-S4). Our SDN-IR analysis inferred the last common crown metazoan ancestor to have emerged 616.9 – 605.9 Ma (early Ediacaran), see Table 1 for a summary of the age inferred for key nodes across all our analyses. Similarly, the sponge last common crown ancestor was dated to 615.3 – 601.3 Ma (early Ediacaran). Crown-group Silicea (Hexactinellida + Demospongiae) was estimated at 591.3 – 570.3 Ma (middle Ediacaran), Lyssacinosida (within Hexactinellida) at 457.3 – 445 Ma (Late Ordovician), and the last common crown ancestor of Calcarea and Homoscleromorpha at 566.5 – 487.6 Ma (late Ediacaran to late Cambrian). Homoscleromorpha was estimated to have originated 429.1 – 228.6 Ma (middle Silurian – Late Triassic), and Calcarea 351.7 – 213.89 Ma (early Carboniferous – Late Triassic). The last common crown demosponge ancestor is estimated at 559.17 – 536.53 Ma (late Ediacaran – early Cambrian), and the last common crown ancestor of the non-spiculated Verongimorpha and Keratosa 521.85 – 430.44 Ma (early Cambrian – middle Silurian). The last common crown ancestor of the spicule-bearing demosponges (Heteroscleromorpha) is estimated to have existed between 521.97 – 515.05 Ma (middle Cambrian), and the last common crown ancestor of the Haplosclerida was inferred at 403.84 – 246.54 Ma (Early Devonian – Middle Triassic). The last common crown ancestor of the rest of the Heteroscleromorpha was inferred to have existed 503.17 – 412.61 Ma (middle Cambrian – Early Devonian). Within Heteroscleromorpha, the freshwater Spongillida separated from the marine Scopalinida 424.69 – 325.85 Ma (late Silurian – late Carboniferous), while the heteroscleromorph lineages (Tetractinellida, Poecilosclerida and Spongillida) diverged, respectively, 299.37 – 231.07 (early Permian – Late Triassic), 236.53 – 199.74 Ma (Late Triassic – Early Jurassic) and 123.21 – 71.52 Ma (Cretaceous).

Phylogenetic relationships at the root of the metazoan tree are uncertain (*2–8*). While recent evidence based on chromosome fusions was suggested to unambiguously support

Ctenophora as the sister of all the other animals (*5*), this result has now been shown to lack statistical robustness (*6*). Accordingly, for our main molecular clock analysis we used a topology where sponges represent the sister of all the other animals. However, as we acknowledge that there is a lack of consensus on early animal relationships (*2–8*), we tested whether using a tree where ctenophores represent the sister of all the other animals influenced the results of our molecular clock analyses (figs. S10-S11 and tables. S5-S6). These analyses showed that the relative relationships of ctenophores and sponges do not affect the timescale of sponge evolution (cf. (*22*)), as the credibility intervals for the divergence times of all key nodes across the two competing phylogenetic hypotheses overlap. When ctenophores are the first branching animal phyla, the age of the sponge last common crown-ancestor is estimated to fall in the interval 616 – 588 Ma, which includes the interval inferred using the phylogeny where Porifera represents the sister of all the other animal phyla (615.3 – 601.3 Ma).

Ancestral state reconstruction of skeletal elements

a) Incorporation of fossils in the phylogenetic framework

To understand the evolutionary history of spicules, we need to consider both extant and fossil taxa, as the distribution of morphological features found in fossils does not necessarily match what is observed in extant lineages. The phylogenetic relationships of many fossil sponges are still debated, which limits their utility in resolving the evolutionary history of spicules. However, the recent description of *H. cantori* (*42*) was accompanied by a formal morphological phylogenetic analysis including extant and fossil taxa. Furthermore, the fossil taxa in (*42*) encompassed a good sampling of the diversity of spicules found in early sponges. This provided us with a means of integrating a sample of fossil sponges (and their spicules) into our analyses. These fossils include the biminerallic *Eiffelia* (*61*) and *Protospongia* (*62*), the siliceous *Cyathophycus*, and the aspiculate *H. cantori* (*42*). Finally, the fossils in the dataset include *Vauxia,* a Cambrian sponge initially described as a non-mineralized demosponge (*63*) that has since been shown to possess silicified fibres (*42*, *44*, *64*) if not spicules (*65*). Phylogenetically, *Vauxia* is now considered a stem silicean (*42*). In order to confirm the placement of these fossils within the context of the tree in Fig. 1, we reanalyzed the matrix of (*42*) using partial constraints to ensure the resulting topology was consistent with our phylogenomic tree while allowing fossil placements to be informed by the morphological data. Our results only differed from those of (*42*), see their Extended Data Figure 5b, because we recovered *Vauxia* in a polytomy at the base of Porifera, rather than as a stem silicean (*42*). To take into consideration the

possibility that *Vauxia* might not be a stem Silicea, we performed ancestral state reconstruction using two topologies: the topology in the Extended Data fig. 5b in (*42*) and the one recovered in our analyses. Both topologies are presented in fig. S12.

b) Ancestral state estimations

We performed three ancestral state estimation using Structured Markov Models with embedded dependencies (*45*). One used the topology in Fig. 1 and did not include fossils. The other two used the topologies in fig. S12 and included fossils (see above, Materials and Methods and Supplementary Methods in SM for details). All analyses, irrespective of whether they included fossils and irrespective of the placement of *Vauxia* (Fig. 2 and fig. S13), suggest that the last common crown-ancestor of Porifera, as well as the last common crown-ancestor of Calcarea plus Homosleromorpha, were not biomineralized (P≥ 0.755 and P≥ 0.726 respectively). Similarly, all but one of our analyses suggested that the last common crown-ancestor of Silicea was not biomineralized (P≥ 0.614). The only exception is the ancestral state reconstruction performed under model B (see Materials and Methods and Supplementary Methods in SM for details) using the tree where *Vauxia* is a stem-group silicean (as in Fig. 2). However, it should be noted that also this analysis did not reconstruct the last common crown-ancestor of Silicea as having possessed spicules. We interpret this result to suggest that under model B, when the tree in Fig. 2 is used, the crown-ancestor of Silicea is reconstructed to have had silicified fibres rather than spicules, similarly to how (*44*) reconstructed *Vauxia*. When biochemical pathway information is incorporated in our models, the probability that all these nodes lacked biomineralization increased (P≥ 0.8). These analyses strongly suggest that spicules were absent in the last common crown-ancestors of sponges (P≥ 0.868) and of Calcarea plus Homosleromorpha (P≥ 0.864). They also suggest that spicules were likely absent in the last common ancestor of total-group Hexactinellida and in the last common crown-ancestor of Demospongiae (P≥ 0.643). Analyses including fossil taxa provide more confidence that the last common crown-ancestor of Porifera lacked spicules (P≥ 0.974). Taken together, the results of our ancestral state estimation analyses suggest that siliceous spicules likely evolved independently a minimum of four times (Fig. 2 and fig. S13), once in Homoscleromorpha, once in Hexactinellida, and twice in Demospongiae (once in the stem Heteroscleromorpha and once in the verongimorph genus *Chondrilla*). When fossil sponges are also considered (Fig. 2 and fig. S13), siliceous spicules emerge independently five times, as we predict an independent origin also in the last common ancestor of *Cyathophycus* and *Minitaspongia* (Fig. 2). Our analyses also strongly support multiple independent origins of

biocalcification. Among the extant taxa in our dataset, biocalcification has evolved once in the stem-lineage of Calcarea and independently in the lineage leading to the demosponge genus *Vaceletia*. When fossil taxa are included, biocalcification is also inferred to have independently evolved in the biminerallic *Eifellia* and in the last common ancestor of the biminerallic *Protospongia* and *Diagoniella* (Fig. 2, fig. S13). All the results of our ancestral state estimations are presented in a separate supplementary result file (Data S1), which is also available in https://figshare.com/s/0a33312af1a00d935f85.

The diversification of Silicea

We tested whether the origin of silicified spicules could have driven adaptive radiations in sponge evolution, performing a case study where we inferred diversification rate shifts in Silicea, the most biodiverse extant sponge lineage. We followed (*66*) and first generated a phylogeny of Silicea performing a constrained ML analysis of 807 *cytochrome c oxidase 1* (COI) barcodes, using our phylogenomic tree (Fig. 1 and fig. S1) to constrain the backbone topology (see Materials and Methods and Supplementary Methods in SM for details). This resulted in a "megaphylogeny" (i.e. a species-rich tree) that was then dated (fig. S14 and table S7; see Materials and Methods and Supplementary Methods in SM for details) and used to perform diversification rate shift analyses using BAMM (*67*) (see table S8 for convergence statistics) and Medusa (*68*), see Materials and Methods and Supplementary Methods in SM for details of how BAMM and Medusa were implemented.

Only one diversification rate shift event was consistently identified by both BAMM and Medusa irrespective of the tree topology used. This shift is placed on the branch leading to the the Axinellida plus Bubarida clade (Fig. 3A-D). A second, putative diversification shift, was identified on the branch leading to Poecilosclerida by all Medusa analyses (Fig. 3B and D) and by one BAMM analysis (BAMM + AR tree; Fig. 3A). Other putative shifts were identified only by individual analyses. One putative shift leading to Hexactinellida was identified by BAMM but only on the IR tree (Fig. 3C), while Medusa identified a putative diversification shifts on the branch leading to Dictyoceratida when using the IR tree (Fig. 3D).

Discussion

The sponge phylogeny is robustly resolved and rooted to the early Ediacaran

The results of our phylogenomic analyses confirm that sponges are split into two fundamental lineages, Calcarea plus Homoscleromorpha, and Demospongiae plus Hexactinellida (Silicea).

Consistent with other phylogenomic and mitogenomic studies (*7*, *8*, *69*), we recovered the monophyly of Keratosa, Verongimorpha and Heteroscleromorpha within Demospongiae. We resolved the aspiculate Keratosa and Verongimorpha as sister clades, and the spiculate Heteroscleromorpha as sister to Keratosa plus Verongimorpha, corroborating previous findings (*69*). The relationships of Bubarida have been a long-standing problem in Demospongiae phylogeny, but our tree recovers Bubarida as the sister of Agelasida+Polymastiida+Tethyida+Clionaida+Suberitida+Poecilosclerida, similar to results recently obtained with mitochondrial genomes (*69*). However, we could not resolve with clear support the relationships of Suberitida with reference to Clionaida, Tethyida, and Poecilosclerida (figs. S1-S3). All our timetrees recover an Ediacaran origin of sponges (615-579 Ma) while rejecting an Ediacaran origin for spiculate demosponges (Heteroscleromorpha; 522-397 Ma), which according to our results cannot be older than Cambrian. While taxon sampling does not allow us to date the origin of Hexactinellida, our results are consistent with recent evidence for a putative crown hexactinellid (*H. cantori*) in the latest Ediacaran (539 Ma (*42*)).

Early sponges did not possess skeletal elements made of silica

Our ancestral character state estimations combined the taxa in our phylogenomic dataset and the fossils in (*42*). All our ancestral state estimate analyses reconstruct the poriferan crown-ancestor and the last common crown-ancestor of Calcarea plus Homoscleromorpha, as not biomineralized and aspiculated ($P > 0.75$). The condition of the silicean crown-ancestor is more uncertain, because of fossil instability (fig. S12) and the fact that for this node, ancestral character state reconstructions are affected by the way in which the embedded dependencies among states are defined (fig. S13). Nonetheless, all our analyses estimate the silicean crown-ancestor as aspiculated ($P > 0.643$), even if the precise probability of this result depends on which tree topology was used to represent the relationships of the fossil taxa (fig. S13), and whether we coded the siliceous spicules of Demospongiae, Homoscleromorpha and Hexactinellida using three different states to reflect biochemical differences. In contrast, the ancestral state estimate of whether the silicean crown-ancestor was capable of biomineralization, depended on tree topology and model combination, with the silicean crown-ancestor emerging as capable of siliceous biomineralization when the tree of (*42*) and model B are used.

If we consider only extant taxa, independent origin of siliceous spicules is suggested in stem-Hexactinellida, Homoscleromorpha (in stem-Plakinidae), in Demospongiae (in stem-

Heteroscleromorpha) and the verongimorph *Chondrilla*. If we count also evolutionary events that happened in extinct lineages, other independent origins of siliceous spicules are inferred. This result is consistent with current interpretations of spicule evolution based on comparative genomics and biochemistry, where developmental and biochemical differences have been interpreted as evidence for the convergent origin of these skeletal structures (*27*, *29*, *30*, *70*), a conclusion that is supported in our study.

Early sponges did not have a calcareous skeleton

Understanding the evolution of calcareous skeletons is more complex. This is because the diversity of calcareous skeletal elements observed across Porifera and their patchy distribution, makes it difficult to decide whether they should be homologised when preparing morphological datasets for ancestral character state estimations. Given that our study was concerned with testing whether the last common crown-ancestor of sponges had skeletal structures, we tested whether early sponges might have had calcareous skeletal elements, irrespective of what these elements were. To achieve our goal, we coded all calcareous skeletal elements found across sponges as homologous. This is a valid hypothesis given that in Metazoa (including sponges) biocalcification is universally reliant on carbonic anhydrase paralogs, which might indicate a homologous origin of biocalcification followed by a diversification process that led to the emergence of significant biochemical and structural differences. However, all our ancestral state reconstructions conclude that calcareous skeletal elements evolved independently in different sponge lineages and were not present in the poriferan crawn-ancestor. Our analyses therefore reject the hypothesis that calcareous skeletal elements in sponges might be homologous and that they were present in the crown-ancestor of all sponges.

Early sponges had low fossilization potential

Given the results of our ancestral state estimation analyses we conclude that latest Ediacaran siliceous spicules were most likely produced by sponges belonging to crown group Silicea, post-dating the origin of crown sponges. Given that stem- and early crown-sponges lacked siliceous spicules and other mineralized skeletal elements, they would have been unlikely to leave fossil remains (*14*). Inevitably, our conclusions are dependent on the sampling of living and fossil sponges included in our ancestral state estimation analyses and our knowledge of their skeletal mineralogy. However, we have attempted to control for this uncertainty by including as many fossil taxa as possible, controlling for the inclusion of states that are not observed in extant lineages: sponges with biminerallic spicules, fossil taxa with

siliceous spicules and siliceous fibres (i.e. biomineralizing but aspiculated), as well as a fossil sponge with no biomineralized skeletal elements. Our results are consistent with the view that the different biochemical pathways used by sponges to produce siliceous spicules represent evidence that the homoscleromorph, hexactinellid and demosponge spicules are not homologous (*27*, *29*, *30*, *70*). In detail, demosponges use silicatein enzymes (*28*, *29*, *71*, *72*) and hexactinellids use glassin, perisilin, and hexaxilin with the organic part of the spicule (the axial filament) having different compositions (*27*, *30*, *73*). Knowledge of the enzymes used by Homoscleromorpha is missing, but homoscleromorphs lack key biosilicification genes found in Hexactinellida and Demospongiae, pointing to a different developmental pathway (*29*, *74*).

The emergence of silicified spicules did not drive the diversification of sponges

Sponges are globally distributed and comprise ca. 9,700 species (*75*). In terms of biodiversity, Demospongiae has undoubtedly been the most successful sponge lineage (*75*). Furthermore, they have been ecologically more successful, for instance being able to transition to freshwater and undergo revolutionary body plan rearrangements, leading to the only known case of carnivory in the phylum (*76*). Many explanations have been proposed to explain their success. One is that the high diversity of spicule shapes would have been advantageous for structural functions and defense, driving adaptive radiations (*77*); the results of our diversification analyses suggest otherwise. While spicules certainly play a role in defense and structural support, their emergence does not appear to have underpinned adaptive radiations, evidence of which should be shown as a diversification event on the branch that leads to the radiation of Heteroscleromorpha. Instead, the only diversification event consistently recovered across all our analyses is on the branch that leads to Bubarida and Axinellida (Fig. 3). Both groups are nested well within Heteroscleromorpha, and spicules were not an innovation specific to them. Furthermore, their spicule types are shared across many other demosponge orders (table S9) where we did not identify diversification events. Analyses that used Medusa highlighted also a putative diversification event in stem-Poecilosclerida, which is however only confirmed by one BAMM analysis and is therefore less certain. Poecilosclerida represents the most speciose demosponge order with ca. 2,488 species described to date (*75*), with a worldwide distribution and substantial ecological diversity. However, Poecilosclerida are also members of the spiculate lineage and did not evolve spicules independently, although they do present one of the largest spicule complements in Porifera. We therefore conclude that while the poecilosclerid evolutionary success might have been linked to the massive expansion of

microscleres observed in this clade (*78*, *79*), the origin of spicules itself cannot have driven their diversification.

Reconciling the fossil record of sponges with molecular estimates of divergence times

Previous evolutionary timelines based on molecular data have inferred sponges to have originated in the Cryogenian (*10*, *12*, *13*, *80*). Differently, our evolutionary timescale infers crown-group sponges to be significantly younger, emerging in the early-middle Ediacaran (617.91–581.39 Ma). Our newly estimated, and younger, clade ages are driven by both a revised geochronology and reinterpretation of the fossil evidence used in establishing calibrations to be used in Bayesian node-dating analyses (*22*). There are a number of speculative interpretations of fossil sponges from the Tonian and Cryogenian but none of these are credible (*14*, *15*). In particular, steranes (24-ipc and 26-mes) found from the late Cryogenian (660–635 Ma) to the Early Cambrian have had a long history of alternative interpretations (*9*, *11*, *81–83*), with the most recent study suggesting they might represent diagenetic derivatives of C_{29} sterols from chlorophyte algae (*18*). Interpreting steranes biomarkers as demosponge-specific would have material implications on our evolutionary timescale. However, ambiguity over their origin implies that, unless new evidence emerges, they should not be used to calibrate molecular clock analyses.

Understanding the siliceous spicule fossil record and reconciling its history against the timescale of sponge evolution is key to elucidating sponge origins. Silica is chemically stable under low-temperature and high-pressure conditions (*14*). If sponges bearing siliceous spicules existed in the Neoproterozoic, they should have been preserved, given also that the Neoproterozoic ocean geochemistry was conductive to the preservation of silica, as confirmed by the presence of abundant cherts in the late Ediacaran (*84*, *85*). The probability that sponges bearing siliceous spicules existed significantly earlier than the oldest known records (ca. 543 Ma) but were not preserved is therefore low (*14*, *25*, *26*). However, the interpretation of the siliceous spicule record is difficult. The oldest siliceous spicules could be interpreted to represent evidence for spicule-bearing stem sponges, in which case the siliceous spicule record would place a limit on the age of crown-sponges, which would be unlikely to be much older than the oldest record of fossil spicules (*14*). However, these spicules can also be interpreted to represent Neoproterozoic evidence for one of the crown lineages bearing siliceous spicules: i.e. Silicea or Homoscleromorpha (although this latter is unlikely (*14*), in agreement with our molecular clock results – Fig. 1). Under this second interpretation, the oldest spicule record would not be representative of the age of the oldest sponges. If the ancestors of these spicule-

bearing crown sponges were aspiculated and not capable of biomineralizing, they would have had low fossilization potential, and would have been unlikely to leave a fossil record (*26*). Under this second hypothesis Porifera could have enjoyed a long, cryptic, Neoproterozoic history, potentially extending to the Cryogenian or the Tonian.

Our analyses did not use the Cryogenian-to-Cambrian fossil biomarkers to calibrate our molecular clock analyses. However, our results still indicate that total-group sponges have a Neoproterozoic history, albeit extending only to the early-middle Ediacaran (617.91–581.39 Ma), that is unrepresented in the fossil record. Accordingly, we shorten the gap between the earliest unambiguous fossil evidence for sponges and molecular divergence times from ca. 150 Myr to 38–75 Myr but continue to support a cryptic phase in the early history of Porifera. Our ancestral character state estimates indicate that stem sponges were aspiculated and uncapable of biomineralization. This allows us to rationalize the Neoproterozoic gap between our molecular estimate for the origin of sponges and the siliceous spicule fossil record as a consequence of the low preservation probability of aspiculated, non-biomineralized, stem-and early crown-sponges.

In accordance with the fossil record, our results suggest that demosponge spicules emerged in ca. 31 Myr interval between 548–517 Ma (Fig. 1). In Homoscleromorpha, silicified spicules were only acquired by the Plakinidae, after the divergence from Oscarellidae in the Carboniferous. Inadequate taxon sampling prevents us from defining precisely the period during which spicules emerged in Hexactinellida. It could be tempting to interpret the aspiculate *H. cantori* to inform a maximum bound on the evolution of spicules in Hexactinellida. However, the diversity of skeletal structures observed in stem hexactinellids (Fig. 2) and the detailed relationships of *H. cantori* within total group Hexactinellida (Fig. 2) suggest that using the age of *H. cantori* as a maximum bound on the origin of siliceous spicules in Hexactinellida would be unwarranted.

Phylogenetic bracketing implies that hexactinellid spicules cannot be older than the silicean crown-ancestor (577.48–561.72 Ma), from which both the Hexactinellida and Demospongiae total-groups emerged. However, siliceous spicules emerged relatively late in demosponges (Fig. 2), potentially suggesting that Hexactinellida might have been the first, among the lineages of extant sponges, to evolve spicules.

Our results explain the existence of an early siliceous spicule fossil record without the need to assume that stem sponges synthesized siliceous spicules. Since sponges branch early within the animal phylogeny (irrespective of the current controversy on the relative relationships between sponges and ctenophores (*2–8*)), they are informative of early metazoan

evolution, and the origin of animal multicellularity. Advocates of a literal reading of the fossil record would suggest that the origin of sponges (and Metazoa) corresponds closely with the first appearance of siliceous spicules in the fossil record (ca. 543 Ma; latest Ediacaran (*15*)). Our divergence time analyses reduce by more than half the perceived gap between the earliest fossil spicules and molecular estimates for the origin of sponges. This gap might diminish even further if older, unambiguous, sponge fossils are discovered. While we agree on the importance of fossils for inferring character evolution and resolving phylogenetic controversies (*86*, *87*), our study demonstrates that the power of the fossil record in inferring evolutionary history is predicated on restoring extinct species to the rightful place within the phylogenies of living taxa. Only with an integrated understanding of phylogeny and character evolution we can hope to achieve an understanding of the evolutionary assembly of animal bodyplans (*88*).

Materials and Methods

Sample collection, RNA extraction, library preparation, Illumina sequencing

Twelve novel sponge specimens were collected for RNA extraction (table S10). Samples were preserved in RNAlater (Thermo Scientific, Waltham, USA) using an overnight incubation at 4°C before long-term storage at -80 °C. Total RNA was extracted with TRIzol (Ambion, Austin, USA) and mRNA purified with a Dynabeads mRNA DIRECT kit (Thermo Scientific, Waltham, USA). The cDNA libraries were constructed with either the kits TruSeq v2 or Scriptseq v2 RNA Library Prep kit (Illumina), according to the manufacturer's instructions, using the maximum quantity of mRNA allowed, which was 50ng – 100ng of starting material. The quality of the libraries was checked with an Agilent TapeStation 2200 system (Agilent Technologies) and the quantity with Qubit™ dsDNA HS Assay kit (ThermoFisher Scientific). The sequencing was conducted with an Illumina NextSeq 500 platform at the Sequencing Facilities of the Natural History Museum of London (Research Core Labs), using a paired-end read strategy (bp length: 2x150 bp).

Assembly of transcriptomic data and extraction of the phylogenomic dataset.

In addition to the 12 novel transcriptomes, 58 published RNA-seq data sets with Sequence Read Archive (SRA) IDs were included. All data were translated to proteins with the final total dataset composed of 70 proteomes (table S10). See Supplementary Methods is SM for details about the software and settings used in the analyses.

Orthologs were inferred using an Orthofinder (*49*) based pipeline, see Supplementary Methods is SM for details about the software and settings used in the pipeline. The final dataset generated in this way was composed of 133 genes that were analysed independently to reconstruct gene trees in IQTree (*50*) and concatenated in a super-alignment of 103,296 AA using the catfasta2phyml.pl script from https://github.com/nylander/catfasta2phyml.

Phylogenetic analyses

The 103,296 AA superalignment was analysed using Maximum Likelihood (ML) in IQTree2 v2.1.3 (*89*). Model testing was performed using the BIC in IQTree2, considering only across-site compositionally homogeneous models. Model selection identified the Q.INSECT+I+G4 model as best fit. We used the ultrafast bootstrap (1,000 replicates) to estimate support for the nodes in the ML tree. Bayesian analyses were performed using Phylobayes (*52*) under the across-site compositionally-heterogeneous CAT-Poisson model (*51*). In these analyses support values are estimated using Posterior Probabilities (PP). We ran two independent chains for over 7,000 generations (Burnin = 1500). Convergence was tested using *Bpcomp* (maxdiff = 0.0018315) and *Tracecomp* (minimal ESS 61 and maximum real_diff= 0.224488). *Bpcomp* and *Tracecomp* are part of the Phylobayes distribution (See table S8 for full convergence scores). Finally we used ASTRAL (*53*) as a coalescent tree reconstruction method on the 133 gene trees generated from the ML analyses of the single gene alignments, performed in IQTree under their gene-specific best fitting model – see Supplementary Methods in SM for details. Astral was used with default parameters.

Inference of divergence times

We fixed the tree topology to our inferred Bayesian tree (Fig. 1 and figs. S3) and constrained the age of 12 nodes representing major sponge clades in our phylogeny (red dots and circles in Fig. 1) based on fossil evidence (see "List of Calibrations and their Justifications" in SM). The oldest fossil spicule was initially used to calibrate the origin of the Spicule-bearing Demospongiae (SDN calibration strategy). We used a uniform prior on the root age with a soft maximum of 609 Ma (pU= 0.025) and a hard minimum of 574 Ma (p= 1e-300; this small value enables the usage of hard bounds in MCMCtree as pL= 0 would cause numerical underflow). We constrained the age of Eumetazoa with a hard maximum of 573 Ma (pU = 1e-300) and a soft minimum of 561 Ma (pU = 0.025) to avoid truncation issues during the MCMC runs (*86*). The age of the other ten calibrated nodes was constrained using heavy-tail Cauchy distributions (i.e., lower-bound calibrations with an offset of p= 0.1 or p= 0.5, a scale parameter of c= 0.5

or c= 0.1, and a left tail probability of pL= 1e-300 to enforce a hard bound on the specified minimum age). The use of a heavy-tailed distribution was preferred as it allows us to capture the credibility of the sponge fossil record, which is unlikely to be reliable in deep time because of taphonomic processes having altered diagnostic characters, thus posing further difficulties on taxonomic classifications. We performed a sensitivity test (SPN strategy) where the oldest siliceous spicule was reassigned to calibrate the node representing the last common sponge ancestor (see also Fig. 1) to account for the uncertainty in the spicule fossil record, allowing us to investigate its impact on poriferan divergence times derived from a molecular clock-dating analysis. In short, the SDN strategy constrained the spicule bearing Demospongiae (Heteroscleromorpha) to have a hard minimum at 515 Ma, while the SPN strategy constrained the root of Porifera to a minimum age of 515 Ma. Both experiments used a Cauchy distribution specified in the same way (c= 0.5, p = 0.5, and pL=1e-300). The age of 515 Ma used in both the SDN and SPN strategies is based on loose siliceous spicules from the lower Cambrian (Series 2, Stage 3) Sirius Passet Biota of North Greenland (*90*). A list of all the calibrations used can be found in the SM – List of Calibrations and their Justifications.

To estimate species divergence times, we dated our inferred Bayesian phylogeny (fig. S1) using MCMCtree, which is part of the PAML package (86). See Supplementary Methods is SM and https://doi.org/10.5281/zenodo.11488993 for details about the settings of all our molecular clock analyses.

To account for uncertainty on sponge divergence that might be caused by phylogenetic uncertainty at the root of the animal tree of life, we ran a ML analysis constraining the topology to force Ctenophora to represent the sister group of all the other animals. We then calibrated the ML tree using the same calibrations used in our other molecular clock analyses and performed new divergence time analyses. We used our in-house pipeline for chains filtering and to generate convergence and summary plots (see above, SM and fig. S15 to S17).

There is some disagreement on the nature of *Geoditesia jordaniensis* (*91*). Accordingly, we performed a sensitivity analysis where we changed the calibration interval defined by this fossil (166.1–163.5 Ma), to 166.1–150 Ma, to take into consideration uncertainty on this part of the sponge fossil record. This analysis did not affect our results.

Ancestral Character State Reconstructions

a) Assembling a phylogenetic framework with fossils and extant taxa

Sponges have a rich fossil record (*14*), which can provide additional evidence of spicule evolution. Fossil observations are particularly useful for ancestral state estimation, as their

closer proximity to the root of the phylogenetic tree compared to living taxa gives them greater influence on ancestral likelihoods. Unfortunately, the majority of fossil sponges have never been included in a formal phylogenetic analysis and their relationships are unknown. However, the recent study of the relationships of *H. cantori* (*42*), included a good selection of fossil sponges. Crucially, this study included fossil taxa with a broad diversity of skeletal structure, from the aspiculate and non-biomineralised *H. cantori* itself to the biminerallic *Eiffelia* and *Protospongia,* and the silicified but most likely aspiculated *Vauxia*. In order to test the effect of fossils on our ancestral states analyses, we produced time trees from phylogenies integrating the results of phylogenomic analysis with those of (*42*). While our main ancestral state reconstruction analysis used the tree published by (*42*) in Extended Fig. 5b, we tested the results of the analyses of (*42*) performing new partially constrained Bayesian analyses (in MrBayes 3.7 (*92*)) were we left the fossils free to arrange themselves in the optimal position in a backbone tree representing by our phylogenomic results. That is, on a tree constraining the monophyly of Silicea (Hexactinellida plus Demospongiae) and that of Calcarea plus Homoscleromoprha. Methodological details of these analyses are presented in Supplementary Methods is SM. Input and result files for these analyses, which identified a placement of the fossil *Vauxia* which is slightly different from that of (*42*), see results above, are also available https://figshare.com/s/0a33312af1a00d935f85. Because our phylogenetic results were slightly different from those of (*42*), we performed a sensitivity analysis were we used the topology inferred from our reanalysis of the dataset of (*42*) (reported in Fig. S12), rather than the tree presented by (*42*) in Extended Fig. 5b, for our ancestral state reconstructions.

b) Estimation of ancestral states

We performed marginal likelihood ancestral state estimation in R, see Supplementary Methods is SM and https://figshare.com/s/0a33312af1a00d935f85 for details of packages and functions used. Character states for the full dataset were sourced from the literature (table S9). The matrix we used for the analyses can be downloaded: https://figshare.com/s/0a33312af1a00d935f85. To investigate the evolution of different spicule types, we used Embedded Dependency Models (*45*) and accounted for underlying biochemical and developmental differences and similarities.

We coded the following characters:

1. Spicule presence: absent = 0, present = 1
2. Calcareous biomineralisation: absent = 0, present = 1

3. Siliceous biomineralisation: absent = 0, present = 1
4. Siliceous spicule mineralisation pathway: Hexactinellida = 0; Demospongiae = 1; Homoscleromorpha = 2

For calcareous spicules, we did not differentiate developmental pathways, assuming a shared mechanism across taxa. This assumption reflects the widespread use of carbonic anhydrase paralogs in sponges to form carbonate-based skeletal elements, including spicules (*31*, *32*, *37*, *38*). The use of carbonic anhydrase paralogs can be considered a shared similarity that could underpin a relationship of homology across all calcified skeletal elements in sponges. It is important to stress that we are aware of the significant differences in biocalcification pathways across sponges (*32*) and we do not propose that biocalcified skeletal elements found across Porifera are homologous. We simply define a putative homology across these structure (an hypothesis of homology) that we then test using ancestral character estimation.

Characters (ii) and (iii) were treated as independent to accommodate fossil taxa with biminerallic spicules (e.g., *Eiffelia*, *Protospongia* (*41*, *62*)). Character (i) was also treated as independent from (ii) and (iii), allowing for biomineralising taxa that lack spicules (e.g., *Vaceletia*, *Vauxia*(*33*)). Character (iv) was treated as dependent on character (iii), as it reflects alternative biochemical pathways for silica deposition.

See Supplementary Methods is SM for details about how we amalgamated the rate matrices of independent characters using structured Markov models (*45*), and dependent characters using embedded dependencies (*46*). In total, we conducted 432 ancestral state estimations. All analysis scripts are available at: https://figshare.com/s/0a33312af1a00d935f85.

Silicean Diversification Rates through Time

Macroevolutionary dynamics of diversification was modelled using Bayesian Analysis of Macroevolutionary Mixtures (BAMM) v.2.5.0 (*67*) and Medusa (*68*) on large, dated, phylogenies (i.e. megaphylogenies) of the Silicea. We followed (*66*) and first generated a dated megaphylogeny of Silicea performing a constrained ML analysis of 807 *cytochrome c oxidase 1* (COI) barcodes, using our phylogenomic tree as a backbone constraint. We then dated the megaphylogeny of Silicea under the IR and AR molecular clock models using the calibrations in table S12. BAMM and Medusa were then applied on the dated megaphylogenies to infer

diversification rate shifts, see Supplementary Methods is SM for the settings of our BAMM and Medusa analyses.

References

1. J. R. Pawlik, S. E. McMurray, The Emerging Ecological and Biogeochemical Importance of Sponges on Coral Reefs. *Annual Review of Marine Science* **12**, 315–337 (2020).

2. C. W. Dunn, A. Hejnol, D. Q. Matus, K. Pang, W. E. Browne, S. A. Smith, E. Seaver, G. W. Rouse, M. Obst, G. D. Edgecombe, M. V. Sørensen, S. H. D. Haddock, A. Schmidt-Rhaesa, A. Okusu, R. M. Kristensen, W. C. Wheeler, M. Q. Martindale, G. Giribet, Broad phylogenomic sampling improves resolution of the animal tree of life. *Nature* **452**, 745–749 (2008).

3. D. Pisani, W. Pett, M. Dohrmann, R. Feuda, O. Rota-Stabelli, H. Philippe, N. Lartillot, G. Wörheide, Genomic data do not support comb jellies as the sister group to all other animals. *Proceedings of the National Academy of Sciences* **112**, 15402–15407 (2015).

4. R. Feuda, M. Dohrmann, W. Pett, H. Philippe, O. Rota-Stabelli, N. Lartillot, G. Wörheide, D. Pisani, Improved modeling of compositional heterogeneity supports sponges as sister to all other animals. *Current Biology* **27**, 3864–3870 (2017).

5. D. T. Schultz, S. H. D. Haddock, J. V. Bredeson, R. E. Green, O. Simakov, D. S. Rokhsar, Ancient gene linkages support ctenophores as sister to other animals. *Nature* **618**, 110–117 (2023).

6. R. R. Copley, Sponges, ctenophores and the statistical significance of syntenies. bioRxiv [Preprint] (2025). https://doi.org/10.1101/2025.05.07.652388.

7. H. Philippe, R. Derelle, P. Lopez, K. Pick, C. Borchiellini, N. Boury-Esnault, J. Vacelet, E. Renard, E. Houliston, E. Quéinnec, C. Da Silva, P. Wincker, H. Le Guyader, S. Leys, D. J. Jackson, F. Schreiber, D. Erpenbeck, B. Morgenstern, G. Wörheide, M. Manuel, Phylogenomics Revives Traditional Views on Deep Animal Relationships. *Current Biology* **19**, 706–712 (2009).

8. P. Simion, H. Philippe, D. Baurain, M. Jager, D. J. Richter, A. Di Franco, B. Roure, N. Satoh, É. Quéinnec, A. Ereskovsky, P. Lapébie, E. Corre, F. Delsuc, N. King, G. Wörheide, M. Manuel, A Large and Consistent Phylogenomic Dataset Supports Sponges as the Sister Group to All Other Animals. *Current Biology* **27**, 958–967 (2017).

9. D. A. Gold, J. Grabenstatter, A. De Mendoza, A. Riesgo, I. Ruiz-Trillo, R. E. Summons, Sterol and genomic analyses validate the sponge biomarker hypothesis. *Proc. Natl. Acad. Sci. U.S.A.* **113**, 2684–2689 (2016).

10. E. A. Sperling, J. M. Robinson, D. Pisani, K. J. Peterson, Where's the glass? Biomarkers, molecular clocks, and microRNAs suggest a 200-Myr missing Precambrian fossil record of siliceous sponge spicules: Sponge biomarkers, molecular clocks and microRNAs. *Geobiology* **8**, 24–36 (2010).

11. J. A. Zumberge, G. D. Love, P. Cárdenas, E. A. Sperling, S. Gunasekera, M. Rohrssen, E. Grosjean, J. P. Grotzinger, R. E. Summons, Demosponge steroid biomarker 26-methylstigmastane provides evidence for Neoproterozoic animals. *Nat Ecol Evol* **2**, 1709–1714 (2018).

12. D. H. Erwin, M. Laflamme, S. M. Tweedt, E. A. Sperling, D. Pisani, K. J. Peterson, The Cambrian Conundrum: Early Divergence and Later Ecological Success in the Early History of Animals. *Science* **334**, 1091–1097 (2011).

13. M. Dohrmann, G. Wörheide, Dating early animal evolution using phylogenomic data. *Sci Rep* **7**, 3599 (2017).

14. J. P. Botting, L. A. Muir, Early sponge evolution: A review and phylogenetic framework. *Palaeoworld* **27**, 1–29 (2018).

15. J. B. Antcliffe, R. H. T. Callow, M. D. Brasier, Giving the early fossil record of sponges a squeeze. *Biological Reviews* **89**, 972–1004 (2014).

16. E. C. Turner, Possible poriferan body fossils in early Neoproterozoic microbial reefs. *Nature* **596**, 87–91 (2021).

17. F. Neuweiler, S. Kershaw, F. Boulvain, M. Matysik, C. Sendino, M. McMenamin, A. Munnecke, Keratose sponges in ancient carbonates – A problem of interpretation. *Sedimentology* **70**, 927–968 (2023).

18. I. Bobrovskiy, J. M. Hope, B. J. Nettersheim, J. K. Volkman, C. Hallmann, J. J. Brocks, Algal origin of sponge sterane biomarkers negates the oldest evidence for animals in the rock record. *Nature Ecology & Evolution* **5**, 165–168 (2021).

19. A. C. Maloof, C. V. Rose, R. Beach, B. M. Samuels, C. C. Calmet, D. H. Erwin, G. R. Poirier, N. Yao, F. J. Simons, Possible animal-body fossils in pre-Marinoan limestones from South Australia. *Nature Geoscience* **3**, 653–659 (2010).

20. Z. Yin, M. Zhu, E. H. Davidson, D. J. Bottjer, F. Zhao, P. Tafforeau, Sponge grade body fossil with cellular resolution dating 60 Myr before the Cambrian. *Proc. Natl. Acad. Sci. U.S.A.* **112** (2015).

21. J. A. Cunningham, A. G. Liu, S. Bengtson, P. C. J. Donoghue, The origin of animals: Can molecular clocks and the fossil record be reconciled? *BioEssays* **39**, e201600120 (2017).

22. E. Carlisle, Z. Yin, D. Pisani, P. C. J. Donoghue, Ediacaran origin and Ediacaran-Cambrian diversification of Metazoa. *Science Advances* **10**, eadp7161 (2024).

23. M. Brasier, O. Green, G. Shields, Ediacarian sponge spicule clusters from southwestern Mongolia and the origins of the Cambrian fauna. *Geology* **25**, 303–306 (1997).

24. Y. Zhang, X. Yuan, L. Yin, Interpreting Late Precambrian Microfossils. *Science* **282**, 1783–1783 (1998).

25. S. Chang, Q. Feng, S. Clausen, L. Zhang, Sponge spicules from the lower Cambrian in the Yanjiahe Formation, South China: The earliest biomineralizing sponge record. *Palaeogeography, Palaeoclimatology, Palaeoecology* **474**, 36–44 (2017).

26. Q. Tang, B. Wan, X. Yuan, A. D. Muscente, S. Xiao, Spiculogenesis and biomineralization in early sponge animals. *Nat Commun* **10**, 3348 (2019).

27. W. R. Francis, M. Eitel, S. Vargas, C. A. Garcia-Escudero, N. Conci, F. Deister, J. L. Mah, N. Guiglielmoni, S. Krebs, H. Blum, S. P. Leys, G. Wörheide, The genome of the reef-building glass sponge *Aphrocallistes vastus* provides insights into silica biomineralization. *R. Soc. open sci.* **10**, 230423 (2023).

28. W. E. G. Müller, A. Krasko, G. L. Pennec, R. Steffen, M. Wiens, M. S. A. Ammar, I. M. Müller, H. C. Schröder, "Molecular Mechanism of Spicule Formation in the Demosponge Suberites domuncula: Silicatein-Collagen-Myotrophin" in *Silicon Biomineralization*, W. E. G. Müller, Ed. (Springer Berlin Heidelberg, Berlin, Heidelberg, 2003; http://link.springer.com/10.1007/978-3-642-55486-5_8)vol. 33 of *Progress in Molecular and Subcellular Biology*, pp. 195–221.

29. A. Riesgo, M. Maldonado, S. López-Legentil, G. Giribet, A Proposal for the Evolution of Cathepsin and Silicatein in Sponges. *J Mol Evol* **80**, 278–291 (2015).

30. K. Shimizu, M. Nishi, Y. Sakate, H. Kawanami, T. Bito, J. Arima, L. Leria, M. Maldonado, Silica-associated proteins from hexactinellid sponges support an alternative evolutionary scenario for biomineralization in Porifera. *Nature Communications* **15**, 181 (2024).

31. O. Voigt, M. V. Wilde, T. Fröhlich, B. Fradusco, S. Vargas, G. Wörheide, Genetic parallels in biomineralization of the calcareous sponge Sycon ciliatum and stony corals. bioRxiv [Preprint] (2025). https://doi.org/10.1101/2025.02.06.636789.

32. O. Voigt, M. Adamska, M. Adamski, A. Kittelmann, L. Wencker, G. Wörheide, Spicule formation in calcareous sponges: Coordinated expression of biomineralization genes and spicule-type specific genes. *Sci Rep* **7**, 45658 (2017).

33. G. Wörheide, A hypercalcified sponge with soft relatives: Vaceletia is a keratose demosponge. *Molecular Phylogenetics and Evolution* **47**, 433–438 (2008).

34. J. Jeon, M. Simonet Roda, Z.-Y. Chen, C. Luo, S. Kershaw, D. Kim, J.-Y. Ma, J.-H. Lee, Y.-D. Zhang, Phosphatic stromatoporoid sponges formed reefs ~480 Mya. *Proceedings of the National Academy of Sciences* **122**, e2426105122 (2025).

35. P. U. Gilbert, K. D. Bergmann, N. Boekelheide, S. Tambutté, T. Mass, F. Marin, J. F. Adkins, J. Erez, B. Gilbert, V. Knutson, Biomineralization: Integrating mechanism and evolutionary history. *Science advances* **8**, eabl9653 (2022).

36. D. J. Jackson, L. Macis, J. Reitner, B. M. Degnan, G. Wörheide, Sponge Paleogenomics Reveals an Ancient Role for Carbonic Anhydrase in Skeletogenesis. *Science* **316**, 1893–1895 (2007).

37. O. Voigt, B. Fradusco, C. Gut, C. Kevrekidis, S. Vargas, G. Wörheide, Carbonic Anhydrases: An Ancient Tool in Calcareous Sponge Biomineralization. *Front Genet* **12**, 624533 (2021).

38. O. Voigt, M. Adamski, K. Sluzek, M. Adamska, Calcareous sponge genomes reveal complex evolution of α-carbonic anhydrases and two key biomineralization enzymes. *BMC Evolutionary Biology* **14**, 230 (2014).

39. J. Germer, K. Mann, G. Wörheide, D. J. Jackson, The Skeleton Forming Proteome of an Early Branching Metazoan: A Molecular Survey of the Biomineralization Components Employed by the Coralline Sponge Vaceletia Sp. *PLOS ONE* **10**, e0140100 (2015).

40. S. M. Rowland, Archaeocyaths—a history of phylogenetic interpretation. *Journal of Paleontology* **75**, 1065–1078 (2001).

41. J. P. Botting, N. J. Butterfield, Reconstructing early sponge relationships by using the Burgess Shale fossil Eiffelia globosa, Walcott. *Proceedings of the National Academy of Sciences* **102**, 1554–1559 (2005).

42. X. Wang, A. G. Liu, Z. Chen, C. Wu, Y. Liu, B. Wan, K. Pang, C. Zhou, X. Yuan, S. Xiao, A late-Ediacaran crown-group sponge animal. *Nature* **630**, 905–911 (2024).

43. B. Runnegar, J. G. Gehling, S. Jensen, M. R. Saltzman, Ediacaran paleobiology and biostratigraphy of the Nama Group, Namibia, with emphasis on the erniettomorphs, tubular and trace fossils, and a new sponge, Arimasia germsi n. gen. n. sp. *Journal of Paleontology* **98**, 1–59 (2024).

44. F. Wei, Y. Zhao, A. Chen, X. Hou, P. Cong, New vauxiid sponges from the Chengjiang Biota and their evolutionary significance. *Journal of the Geological Society* **178**, jgs2020-162 (2021).

45. S. Tarasov, Integration of Anatomy Ontologies and Evo-Devo Using Structured Markov Models Suggests a New Framework for Modeling Discrete Phenotypic Traits. *Systematic Biology* **68**, 698–716 (2019).

46. S. Tarasov, New Phylogenetic Markov Models for Inapplicable Morphological Characters. *Systematic Biology* **72**, 681–693 (2023).

47. N. Shubin, C. Tabin, S. Carroll, Deep homology and the origins of evolutionary novelty. *Nature* **457**, 818–823 (2009).

48. S. Tarasov, The Invariant Nature of a Morphological Character and Character State: Insights from Gene Regulatory Networks. *Systematic Biology* **69**, 392–400 (2020).

49. D. M. Emms, S. Kelly, OrthoFinder2: fast and accurate phylogenomic orthology analysis from gene sequences. *BioRxiv* **466201** (2018).

50. B. Q. Minh, H. A. Schmidt, O. Chernomor, D. Schrempf, M. D. Woodhams, A. von Haeseler, R. Lanfear, IQ-TREE 2: New Models and Efficient Methods for Phylogenetic Inference in the Genomic Era. *Molecular Biology and Evolution* **37**, 1530–1534 (2020).

51. N. Lartillot, H. Philippe, A Bayesian Mixture Model for Across-Site Heterogeneities in the Amino-Acid Replacement Process. *Molecular Biology and Evolution* **21**, 1095–1109 (2004).

52. N. Lartillot, N. Rodrigue, D. Stubbs, J. Richer, PhyloBayes MPI: Phylogenetic Reconstruction with Infinite Mixtures of Profiles in a Parallel Environment. *Systematic Biology* **62**, 611–615 (2013).

53. S. Mirarab, R. Reaz, Md. S. Bayzid, T. Zimmermann, M. S. Swenson, T. Warnow, ASTRAL: genome-scale coalescent-based species tree estimation. *Bioinformatics* **30**, i541–i548 (2014).

54. Z. Yang, PAML 4: Phylogenetic Analysis by Maximum Likelihood. *Molecular Biology and Evolution* **24**, 1586–1591 (2007).

55. F. S. Dunn, A. G. Liu, D. V. Grazhdankin, P. Vixseboxse, J. Flannery-Sutherland, E. Green, S. Harris, P. R. Wilby, P. C. Donoghue, The developmental biology of Charnia and the eumetazoan affinity of the Ediacaran rangeomorphs. *Science advances* **7**, eabe0291 (2021).

56. C. Yang, Y. Li, D. Selby, B. Wan, C. Guan, C. Zhou, X.-H. Li, Implications for Ediacaran biological evolution from the ca. 602 Ma Lantian biota in China. *Geology* **50**, 562–566 (2022).

57. P. R. Wilby, J. N. Carney, M. P. Howe, A rich Ediacaran assemblage from eastern Avalonia: evidence of early widespread diversity in the deep ocean. *Geology* **39**, 655–658 (2011).

58. S. R. Noble, D. J. Condon, J. N. Carney, P. R. Wilby, T. C. Pharaoh, T. D. Ford, U-Pb geochronology and global context of the Charnian Supergroup, UK: constraints on the age of key Ediacaran fossil assemblages. *Bulletin* **127**, 250–265 (2015).

59. J. L. Thorne, H. Kishino, I. S. Painter, Estimating the rate of evolution of the rate of molecular evolution. *Mol Biol Evol* **15**, 1647–1657 (1998).

60. B. Rannala, Z. Yang, Inferring speciation times under an episodic molecular clock. *Syst Biol* **56**, 453–466 (2007).

61. C. D. Walcott, Middle Cambrian Spongiae. *Smithsonian Miscellaneous Collections* (1917).

62. J. W. Salter, On some new fossils from the lingula-flags of Wales. *Quarterly Journal of the Geological Society of London* **20**, 233–241 (1864).

63. R. M. Finks, R. L. Kaesler, J. K. Rigby, Paleozoic demospongea: morphology and phylogeny. *Treatise on Invertebrate Paleontology, Pt. E, Porifera (revised)* **2**, 63–80 (2003).

64. C. Luo, F. Zhao, H. Zeng, The first report of a vauxiid sponge from the Cambrian Chengjiang Biota. *Journal of Paleontology* **94**, 28–33 (2020).

65. X.-L. Yang, Y.-L. Zhao, L. E. Babcock, J. Peng, Siliceous spicules in a vauxiid sponge (Demospongia) from the Kaili Biota(Cambrian Stage 5), Guizhou, South China. *Sci Rep* **7**, 42945 (2017).

66. M. B. DeBiasse, A. Buckenmeyer, J. Macrander, L. S. Babonis, B. Bentlage, P. Cartwright, C. Prada, A. M. Reitzel, S. N. Stampar, A. G. Collins, A cnidarian phylogenomic tree fitted with hundreds of 18S leaves. *bioRxiv*, 2022–10 (2022).

67. D. L. Rabosky, Automatic Detection of Key Innovations, Rate Shifts, and Diversity-Dependence on Phylogenetic Trees. *PLOS ONE* **9**, e89543 (2014).

68. M. E. Alfaro, F. Santini, C. Brock, H. Alamillo, A. Dornburg, D. L. Rabosky, G. Carnevale, L. J. Harmon, Nine exceptional radiations plus high turnover explain species diversity in jawed vertebrates. *Proceedings of the National Academy of Sciences* **106**, 13410–13414 (2009).

69. D. V. Lavrov, M. C. Diaz, M. Maldonado, C. C. Morrow, T. Perez, S. A. Pomponi, R. W. Thacker, Phylomitogenomics bolsters the high-level classification of Demospongiae (phylum Porifera). *PLOS ONE* **18**, e0287281 (2023).

70. S. Santini, Q. Schenkelaars, C. Jourda, M. Duchesne, H. Belahbib, C. Rocher, M. Selva, A. Riesgo, M. Vervoort, S. P. Leys, The compact genome of the sponge Oopsacas minuta (Hexactinellida) is lacking key metazoan core genes. *BMC biology* **21**, 1–21 (2023).

71. W. E. G. Müller, U. Schloßmacher, C. Eckert, A. Krasko, A. Boreiko, H. Ushijima, S. E. Wolf, W. Tremel, I. M. Müller, H. C. Schröder, Analysis of the axial filament in spicules of the demosponge Geodia cydonium: Different silicatein composition in microscleres (asters) and megascleres (oxeas and triaenes). *European Journal of Cell Biology* **86**, 473–487 (2007).

72. K. Shimizu, J. Cha, G. D. Stucky, D. E. Morse, Silicatein α: Cathepsin L-like protein in sponge biosilica. *Proceedings of the National Academy of Sciences* **95**, 6234–6238 (1998).

73. K. Shimizu, T. Amano, M. R. Bari, J. C. Weaver, J. Arima, N. Mori, Glassin, a histidine-rich protein from the siliceous skeletal system of the marine sponge Euplectella, directs silica polycondensation. *Proceedings of the National Academy of Sciences* **112**, 11449–11454 (2015).

74. M. Maldonado, A. Riesgo, Intra-epithelial spicules in a homosclerophorid sponge. *Cell Tissue Res* **328**, 639–650 (2007).

75. N. de Voogd, B. Alvarez, N. Boury-Esnault, P. Cárdenas, M.-C. Díaz, M. Dohrmann, R. Downey, C. Goodwin, E. Hajdu, J. Hooper, M. Kelly, M. Klautau, S.-C. Lim, R. Manconi, C. Morrow, U. Pinheiro, A. Pisera, P. Ríos, K. Rützler, C. Schönberg, T. Turner, J. Vacelet, R. van Soest, J. Xavier, World Porifera Database. Accessed at https://www.marinespecies.org/porifera on yyyy-mm-dd, VLIZ (2023); https://doi.org/10.14284/359.

76. J. Vacelet, N. Boury-Esnault, Carnivorous sponges. *Nature* **373**, 333–335 (1995).

77. M.-J. Uriz, X. Turon, M. A. Becerro, G. Agell, Siliceous spicules and skeleton frameworks in sponges: Origin, diversity, ultrastructural patterns, and biological functions. *Microscopy Research and Technique* **62**, 279–299 (2003).

78. M. Łukowiak, R. Van Soest, M. Klautau, T. Pérez, A. Pisera, K. Tabachnick, The terminology of sponge spicules. *Journal of Morphology* **283**, 1517–1545 (2022).

79. C. Morrow, P. Cárdenas, Proposal for a revised classification of the Demospongiae (Porifera). *Front Zool* **12**, 7 (2015).

80. M. dos Reis, Y. Thawornwattana, K. Angelis, M. J. Telford, P. C. J. Donoghue, Z. Yang, Uncertainty in the Timing of Origin of Animals and the Limits of Precision in Molecular Timescales. *Curr Biol* **25**, 2939–2950 (2015).

81. J. B. Antcliffe, Questioning the evidence of organic compounds called sponge biomarkers. *Palaeontology*, n/a-n/a (2013).

82. D. A. Gold, S. S. O'Reilly, G. Luo, D. E. G. Briggs, R. E. Summons, Prospects for Sterane Preservation in Sponge Fossils from Museum Collections and the Utility of Sponge Biomarkers for Molecular Clocks. *Bulletin of the Peabody Museum of Natural History* **57**, 181–189 (2016).

83. B. J. Nettersheim, J. J. Brocks, A. Schwelm, J. M. Hope, F. Not, M. Lomas, C. Schmidt, R. Schiebel, E. C. M. Nowack, P. De Deckker, J. Pawlowski, S. S. Bowser, I. Bobrovskiy, K. Zonneveld, M. Kucera, M. Stuhr, C. Hallmann, Putative sponge biomarkers in unicellular Rhizaria question an early rise of animals. *Nat Ecol Evol* **3**, 577–581 (2019).

84. Z. Wang, X. Xie, Z. Wen, Formation conditions of Ediacaran–Cambrian cherts in South China: Implications for marine redox conditions and paleoecology. *Precambrian Research* **383**, 106867 (2022).

85. A. Muscente, F. M. Michel, J. G. Dale, S. Xiao, Assessing the veracity of Precambrian 'sponge'fossils using in situ nanoscale analytical techniques. *Precambrian Research* **263**, 142–156 (2015).

86. M. J. Donoghue, J. A. Doyle, J. Gauthier, A. G. Kluge, T. Rowe, The Importance of Fossils in Phylogeny Reconstruction. *Annual Review of Ecology and Systematics* **20**, 431–460 (1989).

87. C. Patterson, Significance of Fossils in Determining Evolutionary Relationships. *Annual Review of Ecology and Systematics* **12**, 195–223 (1981).

88. K. J. Peterson, R. E. Summons, P. C. Donoghue, Molecular palaeobiology. *Palaeontology* **50**, 775–809 (2007).

89. L.-T. Nguyen, H. A. Schmidt, A. von Haeseler, B. Q. Minh, IQ-TREE: A Fast and Effective Stochastic Algorithm for Estimating Maximum-Likelihood Phylogenies. *Molecular Biology and Evolution* **32**, 268–274 (2015).

90. J. P. Botting, P. Cárdenas, J. S. Peel, A crown-group demosponge from the early Cambrian Sirius Passet Biota, North Greenland. *Palaeontology* **58**, 35–43 (2015).

91. P. Cárdenas, Surface Microornamentation of Demosponge Sterraster Spicules, Phylogenetic and Paleontological Implications. *Front. Mar. Sci.* **7** (2020).

92. F. Ronquist, J. P. Huelsenbeck, M. Teslenko, C. Zhang, J. A. A. Nylander, MrBayes version 3.2 Manual: Tutorials and Model Summaries.

93. Andrews, S, FastQC: a quality control tool for high throughput sequence data., (2010).

94. A. M. Bolger, M. Lohse, B. Usadel, Trimmomatic: a flexible trimmer for Illumina sequence data. *Bioinformatics* **30**, 2114–2120 (2014).

95. M. G. Grabherr, B. J. Haas, M. Yassour, J. Z. Levin, D. A. Thompson, I. Amit, X. Adiconis, L. Fan, R. Raychowdhury, Q. Zeng, Full-length transcriptome assembly from RNA-Seq data without a reference genome. *Nature biotechnology* **29**, 644–652 (2011).

96. L. Fu, B. Niu, Z. Zhu, S. Wu, W. Li, CD-HIT: accelerated for clustering the next-generation sequencing data. *Bioinformatics* **28**, 3150–3152 (2012).

97. K. M. Kocot, M. R. Citarella, L. L. Moroz, K. M. Halanych, PhyloTreePruner: A Phylogenetic Tree-Based Approach for selection of Orthologous sequences for phylogenomics. *Evol Bioinform Online* **9**, EBO.S12813 (2013).

98. S. Whelan, I. Irisarri, F. Burki, PREQUAL: detecting non-homologous characters in sets of unaligned homologous sequences. *Bioinformatics*, doi: 10.1093/bioinformatics/bty448 (2018).

99. R. C. Edgar, MUSCLE: multiple sequence alignment with high accuracy and high throughput. *Nucleic Acids Research* **32**, 1792–1797 (2004).

100. S. Capella-Gutiérrez, J. M. Silla-Martínez, T. Gabaldón, trimAl: a tool for automated alignment trimming in large-scale phylogenetic analyses. *Bioinformatics* **25**, 1972–1973 (2009).

101. J. A. Ballesteros, G. Hormiga, A New Orthology Assessment Method for Phylogenomic Data: Unrooted Phylogenetic Orthology. *Mol Biol Evol* **33**, 2117–2134 (2016).

102. M. dos Reis, Z. Yang, Approximate Likelihood Calculation on a Phylogeny for Bayesian Estimation of Divergence Times. *Molecular Biology and Evolution* **28**, 2161–2172 (2011).

103. H. C. Betts, M. N. Puttick, J. W. Clark, T. A. Williams, P. C. J. Donoghue, D. Pisani, Integrated genomic and fossil evidence illuminates life's early evolution and eukaryote origin. *Nat Ecol Evol* **2**, 1556–1562 (2018).

104. R. J. Howard, M. Giacomelli, J. Lozano-Fernandez, G. D. Edgecombe, J. F. Fleming, R. M. Kristensen, X. Ma, J. Olesen, M. V. Sørensen, P. F. Thomsen, M. A. Wills, P. C. J. Donoghue, D. Pisani, The Ediacaran origin of Ecdysozoa: integrating fossil and phylogenomic data. *Journal of the Geological Society* **179**, jgs2021-107 (2022).

105. K. Angelis, S. Álvarez-Carretero, M. Dos Reis, Z. Yang, An Evaluation of Different Partitioning Strategies for Bayesian Estimation of Species Divergence Times. *Systematic Biology* **67**, 61–77 (2018).

106. L. J. Revell, phytools: an R package for phylogenetic comparative biology (and other things). *Methods in Ecology and Evolution* **3**, 217–223 (2012).

107. M. Pagel, Detecting correlated evolution on phylogenies: a general method for the comparative analysis of discrete characters. *Proceedings of the Royal Society of London. Series B: Biological Sciences* **255**, 37–45 (1997).

108. S. Álvarez-Carretero, A. U. Tamuri, M. Battini, F. F. Nascimento, E. Carlisle, R. J. Asher, Z. Yang, P. C. J. Donoghue, M. dos Reis, A species-level timeline of mammal evolution integrating phylogenomic data. *Nature* **602**, 263–267 (2022).

109. D. L. Rabosky, M. Grundler, C. Anderson, P. Title, J. J. Shi, J. W. Brown, H. Huang, J. G. Larson, BAMMtools: an R package for the analysis of evolutionary dynamics on phylogenetic trees. *Methods in Ecology and Evolution* **5**, 701–707 (2014).

110. J. J. Matthews, A. G. Liu, C. Yang, D. McIlroy, B. Levell, D. J. Condon, A chronostratigraphic framework for the rise of the Ediacaran macrobiota: new constraints from Mistaken Point Ecological Reserve, Newfoundland. *Bulletin* **133**, 612–624 (2021).

111. F. Dunn, C. Kenchington, L. Parry, J. Clark, R. Kendall, P. Wilby, A crown-group cnidarian from the Ediacaran of Charnwood Forest, UK. *Nature Ecology & Evolution* **6**, 1095–1104 (2022).

112. Z. Yin, W. Sun, P. Liu, M. Zhu, P. C. Donoghue, Developmental biology of Helicoforamina reveals holozoan affinity, cryptic diversity, and adaptation to heterogeneous environments in the early Ediacaran Weng'an biota (Doushantuo Formation, South China). *Science advances* **6**, eabb0083 (2020).

113. Z. Yin, K. Vargas, J. Cunningham, S. Bengtson, M. Zhu, F. Marone, P. Donoghue, The early Ediacaran Caveasphaera foreshadows the evolutionary origin of animal-like embryology. *Current Biology* **29**, 4307–4314 (2019).

114. C. Yang, A. D. Rooney, D. J. Condon, X.-H. Li, D. V. Grazhdankin, F. T. Bowyer, C. Hu, F. A. Macdonald, M. Zhu, The tempo of Ediacaran evolution. *Science advances* **7**, eabi9643 (2021).

115. M. Benton, P. Donoghue, J. Vinther, R. Asher, M. Friedman, T. Near, Constraints on the timescale of animal evolutionary history. *Palaeontologia Electronica*, doi: 10.26879/424 (2015).

116. X.-P. Dong, J. A. Cunningham, S. Bengtson, C.-W. Thomas, J. Liu, M. Stampanoni, P. C. Donoghue, Embryos, polyps and medusae of the Early Cambrian scyphozoan Olivooides. *Proceedings of the Royal Society B: Biological Sciences* **280**, 20130071 (2013).

117. F. T. Bowyer, A. Y. Zhuravlev, R. Wood, G. A. Shields, Y. Zhou, A. Curtis, S. W. Poulton, D. J. Condon, C. Yang, M. Zhu, Calibrating the temporal and spatial dynamics of the Ediacaran-Cambrian radiation of animals. *Earth-Science Reviews* **225**, 103913 (2022).

118. M. Steiner, G. Li, Y. Qian, M. Zhu, B.-D. Erdtmann, Neoproterozoic to early Cambrian small shelly fossil assemblages and a revised biostratigraphic correlation of the Yangtze Platform (China). *Palaeogeography, Palaeoclimatology, Palaeoecology* **254**, 67–99 (2007).

119. B. Runnegar, Muscle scars, shell form and torsion in Cambrian and Ordovician univalved molluscs. *Lethaia* **14**, 311–322 (1981).

120. M. Steiner, G. Li, Y. Qian, M. Zhu, Lower Cambrian small shelly fossils of northern Sichuan and southern Shaanxi (China), and their biostratigraphic importance. *Geobios* **37**, 259–275 (2004).

121. H. Mostler, Mikroskleren von demospongien (Porifera) aus dem basalen Jura der nördlichen Kalkalpen. *Geologisch-Paläontologische Mitteilungen Innsbruck* **17**, 119–142 (1990).

122. M. Łukowiak, Fossil and modern sponge fauna of southern Australia and adjacent regions compared: interpretation, evolutionary and biogeographic significance of the late Eocene 'soft'sponges. *Contributions to Zoology* **85**, 13–35 (2016).

123. N. P. James, Y. Bone, Eocene cool-water carbonate and biosiliceous sedimentation dynamics, St Vincent Basin, South Australia. *Sedimentology* **47**, 761–786 (2000).

124. K. A. Ritterbush, S. Rosas, F. A. Corsetti, D. J. Bottjer, A. J. West, Andean sponges reveal long-term benthic ecosystem shifts following the end-Triassic mass extinction. *Palaeogeography, Palaeoclimatology, Palaeoecology* **420**, 193–209 (2015).

125. D. Ungureanu, F. Ahmad, S. Farouk, A Callovian (Middle Jurassic) poriferan fauna from northwestern Jordan: taxonomy, palaeoecology and palaeobiogeography. *Historical Biology* **30**, 577–592 (2018).

126. T. Schindler, M. Wuttke, M. Poschmann, Oldest record of freshwater sponges (Porifera: Spongillina)—spiculite finds in the Permo-Carboniferous of Europe. *Paläontologische Zeitschrift* **82**, 373–384 (2008).

127. S. Fortunato, M. Adamski, B. Bergum, C. Guder, S. Jordal, S. Leininger, C. Zwafink, H. T. Rapp, M. Adamska, Genome-wide analysis of the sox family in the calcareous sponge Sycon ciliatum: multiple genes with unique expression patterns. *Evodevo* **3**, 14 (2012).

Acknowledgments

Funding:

NERC GW4+ PhD studentship (MER).
John Templeton Foundation (62220) (DP, PCJD)
Gordon and Betty Moore Foundation (GBMF9741) (DP, PCJD)
University of Bristol URF fellowship, and a Leverhulme Trust Grant RPG-2024-030 (DP)
Rutherford Discovery Fellowship RDF-UOO2001 from the Royal Society of New Zealand (NJK)
ERC grant no. 788203 (INNOVATION) (JNK)
Villum Fonden grant no. 679849 and EnBie grant no. 54433. (AS)

Author contributions:

DP, AR and PJD conceived the study. MER performed the analyses and wrote the first draft of the paper. DP, PJD and AR edited the paper. MG, NK, and MER performed orthology inference. JNK provided support for the ASE analyses, SAC provided support and scripts for timetree inference analyses. PC and AS provided some of the fossil calibrations and helped assemble the morphological matrix used in the ASE. ST, VK, AR, and PC took part in the sampling. BP, ST, VK, NK and MER extracted the RNA and performed library preparations of the samples.

Competing interests: The authors declare that they have no competing interests.

Data and materials availability: All new RNA-Seq data produced in this study has been deposited in the Sequence Read Archive and all accession numbers have been provided in table S10. Data used for phylogenomic, diversification events, time calibrations, and ancestral state estimation have been deposited in figshare (https://figshare.com/s/0a33312af1a00d935f85). The code and pipelines developed for the time calibration analyses can be found at https://doi.org/10.5281/zenodo.11488993 .

Figures and Tables

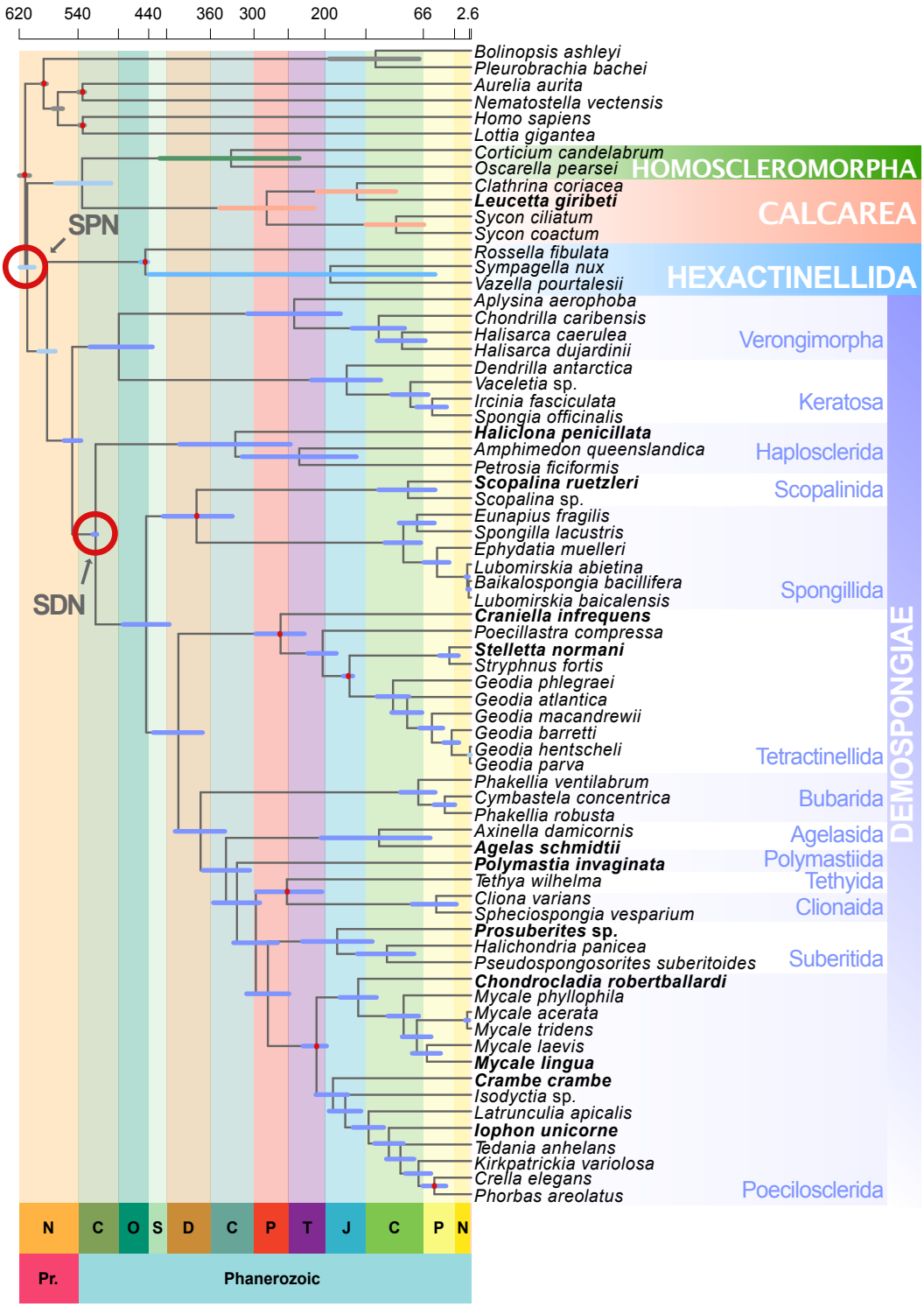

FIGURE 1 Time-calibrated phylogeny dates the origin of sponges to the early Ediacaran Porifera time-tree with posterior estimates using the Spicule-bearing Demospongiae (SDN) calibration strategy (red circle) and the IR model in MCMCtree. Blue bars on nodes represent the 95% HPD. Red circles represent the two mutually exclusive calibrations strategies

Spiculated Porifera Node (SPN) and SDN. Full red dots represent calibrations in both strategies. Species in bold were sequences in the framework of this study. Time scale on x-axis in hundreds of millions of years. Abbreviation on the scale bar stands for Ne, Neoproterozoic; C, Cambrian; O, Ordovician; S, Silurian; D, Devonian; C, Carboniferous; P, Permian; Tr, Triassic; J, Jurassic; K, Cretaceous; Pe, Paleogene. The tree topology represents our Bayesian phylogeny (fig. S1). Support values for the nodes can be found in fig. S1. Differences between our ML, Bayesian and Astral topologies are described in text and can be investigated comparing the tree in Fig.1 against those in fig. S2 and S3.

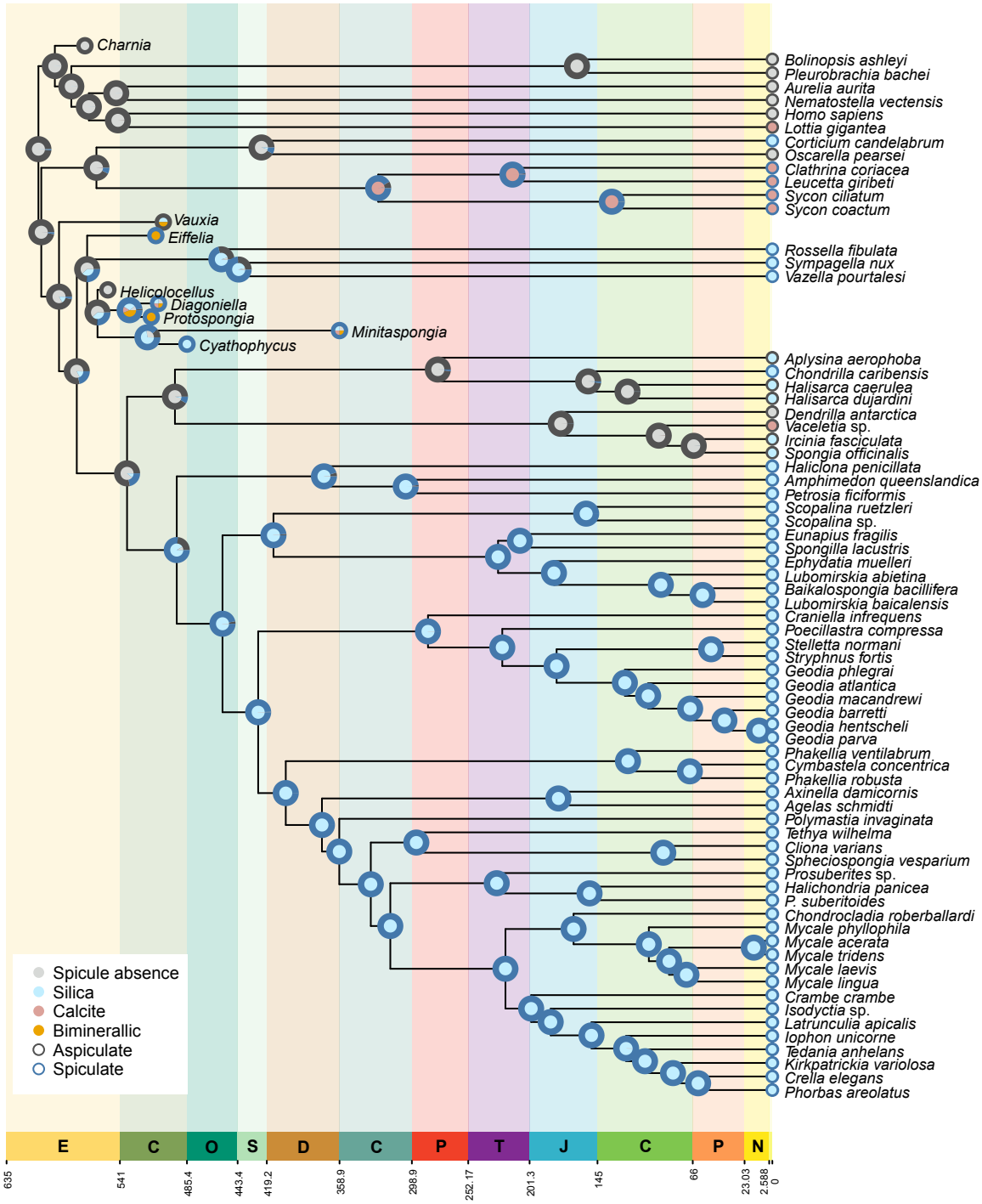

FIGURE 2 Early sponges did not have biomineralized skeletons

Ancestral state estimations of sponge skeletal elements obtained using the tree topology from ((*42*) – Extended Data Fig. 5b) dated using the time-tree inferred using the SDN calibration strategy and the structured Markov model combining the presence/absence of spicules and their mineralogy (Model D). Grey absence of spicules, light blue for siliceous mineralogy, red for calcareous mineralogy, and orange for biminerallic spicules. Outside circles represent the presence (blue) or absence (dark grey) of spicules.

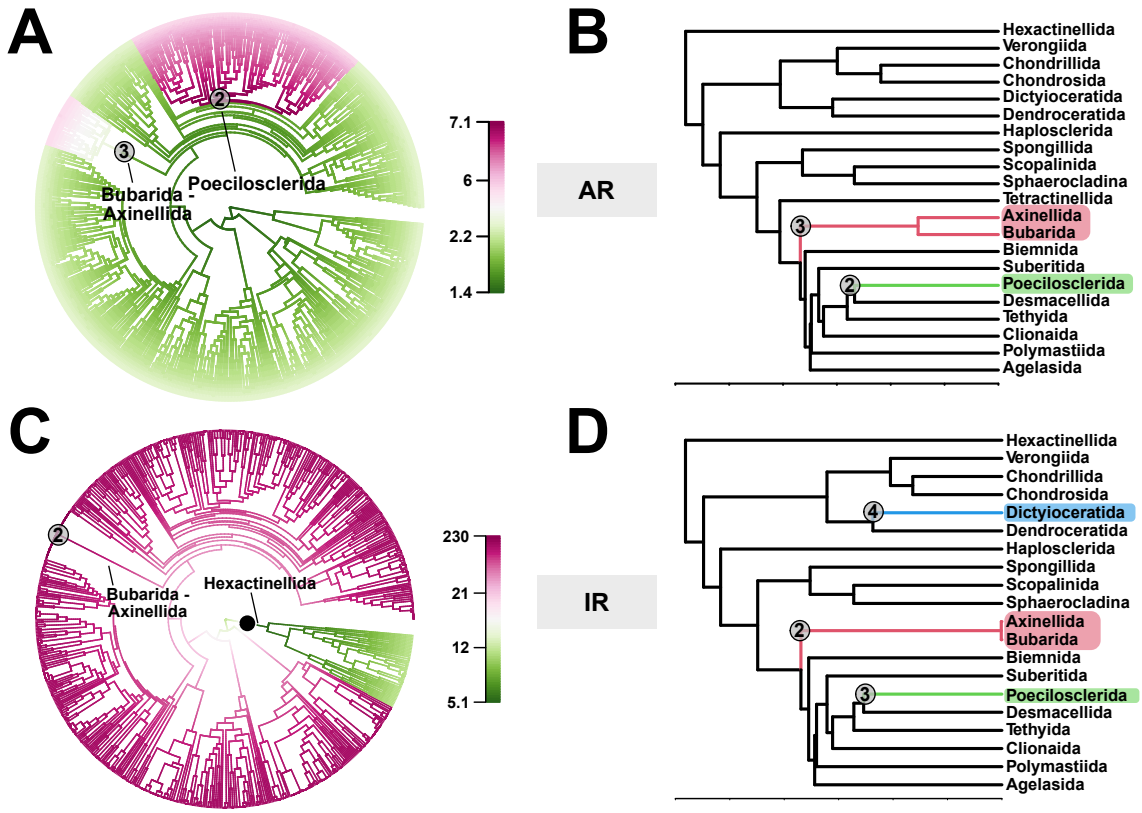

FIGURE 3 Diversifications events in Silicea do not correlate with spicule evolution

Rate diversification tests. Grey dots with numbers correspond to the shift highlighted by both Medusa and BAMM analyses, the same number is reported when the same shift corresponds on both topologies. **(A)** BAMM results for the COI timetree inferred with the AR model. The two shifts highlighted are on the branches of Bubarida + Axinellida (3), and Poecilosclerida (2). **(B)** Medusa results for the subsampled topology obtained with the AR molecular clock model. **(C)** BAMM results for the COI timetree inferred with the IR molecular clock model. The two shifts highlighted are on the branches of Bubarida + Axinellida (2) and Hexacintellida (black full dot). **(D)** Medusa results for the subsampled topology obtained with the IR molecular clock model which highlights diversification rates in Axinellida+ Bubarida(2), Poecilosclerida (3), and Dyctioceratida (4).

Table 1 Summary of posterior mean time estimates under both calibration strategies and molecular clock models for key nodes in our timetree. Full details can be found in tables S3-S4.

Nodes	SDN AR 95% CIs for time estimates	SPN AR 95% CIs for time estimates	SDN IR 95% CIs for time estimates	SDN IR 95% CIs for time estimates
Porifera	603.79-582.68	594.59-578.79	615.32-601.3	610.68-590.34
Silicea	577.48-561.72	567.69-551.55	591.32-570.3	575.87-542.68
Demospongiae	549.57-538.18	535.02-503.38	559.17-536.53	519.67-462.67
Hexactinellida	454.92-445.07	443.89-422.5	457.3-445.09	454.99-445.07
Calcarea	473.24-163.27	460.38-157.52	351.7-213.89	337.36-207.53
Homoscleromorpha	540.28-435.36	535.63-420.18	429.15-228.57	421.58-224.87
Heteroscleromorpha	521.97-515.05	500.69-455.96	520.81-515.04	454.95-396.53